Chapter 1 Effect of simultaneous microwave-ultrasound irradiation on the synthesis of hydrotalcite-derived mixed oxides for As(III) removal

Capítulo 1 Efecto de la irradiación simultánea de microondas-ultrasonido en la síntesis de óxidos mixtos derivados de hidrotalcita para la eliminación de As(III)

GARZÓN-PÉREZ, Amanda Stephanie[1], PAREDES-CARRERA, Silvia Patricia[2], VELÁZQUEZ-HERRERA, Franchescoli Didier[3] and ZARAZUA-AGUILAR, Yohuali[*4]

[1]*Instituto de Metalurgia, Universidad Autónoma de San Luis Potosí*
[2]*Laboratorio de Nanomateriales Sustentables, Escuela Superior de Ingeniería Química e Industrias Extractivas, Instituto Politécnico Nacional*
[3]*Laboratorio de Materiales Bioactivos, Facultad de Ciencias Químicas, Benemérita Universidad Autónoma de Puebla*
[4]*Unidad Académica Profesional Acolman, Universidad Autónoma del Estado de México*

ID 1st Author: *Amanda Stephanie, Garzón-Pérez* / **ORC ID**: 0000-0002-2349-7115, **CVU CONACYT ID:** 742764

ID 1st Co-author: *Silvia Patricia, Paredes-Carrera* / **ORC ID**: 0000-0002-5388-7982, **CVU CONACYT ID:** 37605

ID 2nd Co-author: *Franchescoli Didier, Velázquez-Herrera* / **ORC ID**: 0000-0001-6011-055X, **CVU CONACYT ID:** 488215

ID 3rd Co-author: *Yohuali, Zarazua-Aguilar* / **ORC ID**: 0000-0003-3788-4682, **CVU CONACYT ID:** 447394

DOI: 10.35429/H.2022.8.1.13

A. Garzón, S. Paredes, F. Velázquez and Y. Zarazua

*yzarazuaa@uaemex.mx

A. Marroquín, J. Alonso, Z. Chavero and L. Cruz (Coord) Engineering and Innovation. Handbooks-©ECORFAN-México, Querétaro, 2022.

Abstract

Inorganic arsenic water contamination turns out to be a serious problem worldwide. According to the World Health Organization (WHO), more than 140 million people worldwide consume water with high levels of arsenic, causing diseases such as cancer. Arsenic is found as As^{3+} ($As(OH)_3$) mainly in surface water effluents, which increases the interest in its removal with low-cost materials and regeneration capacity. For this reason, in this chapter, the study of As(III) adsorption on hydrotalcite-derived mixed oxides ZnAl, synthesized by an alternative simultaneous microwave/ultrasound irradiation method, followed by the formation of mixed oxides by calcination. The specific surface area of the calcined sample obtained by simultaneous irradiation was about 59 m^2/g, being higher compared to the individually irradiated materials, ultrasound, and microwaves, 20 and 50 m^2 /g, respectively. This indicated that the increase in the specific surface area was attributed to a synergistic effect promoted by combining the irradiation methods (microwaves-ultrasound). SEM images show that the morphology of the mixed oxides also depends on the irradiation mode used during the hydrotalcite synthesis, generating an arrangement of two phases of particles. Simultaneous irradiation provides a simple way to obtain materials with better textural properties in a short synthesis time and favors a high adsorption capacity (0.52 mg/g), compared to individually irradiated materials.

Synergistic, Synthesis, Mixed oxides, Arsenite, Simultaneous irradiation

1 Introduction

Wastewater from the industrial production of glass, pesticides, pigments, textiles, and metallic adhesives, among others, usually contains inorganic contaminants like heavy metals (copper, aluminum, mercury, cadmium, and arsenic), are toxic in high concentrations and lead to serious health problems, mainly cancer (Sekabira et al., 2010). Therefore, arsenic removal from aqueous effluents is one of the most important challenges for industry and society. In general, treatment technologies are believed to be most effective using a two-step approach, consisting of the initial oxidation of As(III) to As(V), followed by a procedure for As(V) removal. Therefore, one-step As(III) removal is an excellent development for the industry because it can reduce process costs (Mohan & Pittman, 2007; Nicomel et al., 2015).

In recent years, various techniques have been tested for As(III) removal, such as physical-chemical and biological methods, ozonization, catalytic and photocatalytic degradation, and adsorption process. Adsorption is the most widely used removal method, as it is an easily applied technique and does not require the introduction of undesirable anions into the medium (Deschamps et al., 2003; Nicomel et al., 2015). Thus, it can be considered an economical and fast method for As(III) removal because adsorbent materials can be obtained on a large scale with low costs from nature or synthetically. The most commonly used adsorbents today are materials with large surface areas, such as alumina, silica gel, activated carbon, and clays (De Gisi et al., 2016) being anionic clays the most suitable due to their capacity to retain anions and, when calcined, they originate mixed oxides, which can be reconstructed in the initial structure of the hydrotalcite, capturing the anions during this process.

Anionic clays are natural or synthetic clays commonly designed as layered double hydroxides (LDH), hydrotalcite like-compounds or simply designed as hydrotalcites (HT). They are non-toxic, environmentally friendly and relatively inexpensive materials (Velázquez-Herrera, Lobo-Sánchez, et al., 2022). Its structure is similar to the brucite [$Mg(OH)_2$], where some Mg^{2+} atoms can be replaced by trivalent atoms, Figure 1, resulting in a general formula: $[M^{2+}_{1-x}M^{3+}_{x}(OH)_2](A^{m-})_{x/m} \cdot nH_2O$, where M^{2+} corresponds to a divalent cation (Mg^{2+}, Zn^{2+}, Ni^{2+}, Cu^{2+}) and M^{3+} corresponds to a trivalent cation (Al^{3+}, Cr^{3+}, Ga^{3+}, Fe^{3+}). A^{m-} is a compensation anion (CO_3^{2-}, SO_4^{2-}, Cl^-, NO_3^-), and x is the metal molar ratio $M^{3+}/(M^{2+}+M^{3+})$ (Ghashghaee et al., 2018; Nie, 2020; Velázquez-Herrera & Fetter, 2020).

Figure 1 Hydrotalcite structure representation

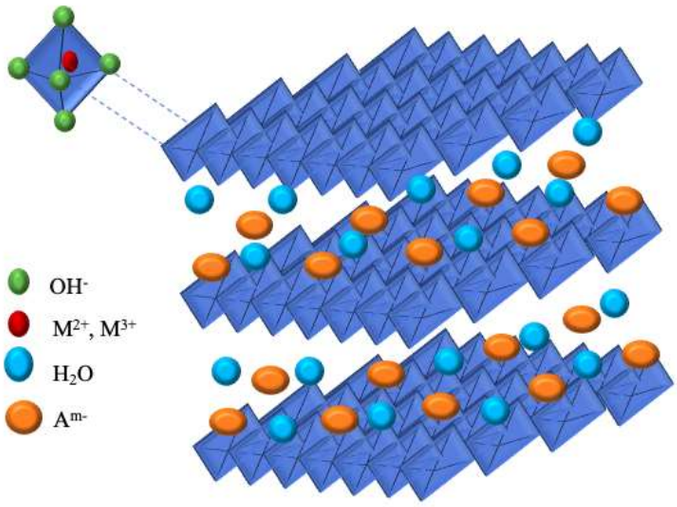

Source: "By the Authors"

As hydrotalcites are scarce in nature, they are usually synthesized through different methods such as coprecipitation, sol-gel, and urea hydrolysis (Conterosito et al., 2018; Lima-Corrêa et al., 2018). The most common method is coprecipitation at constant pH, followed by a crystallization step that can be proceeded by hydrothermal treatments in autoclaves or microwave or ultrasound irradiations apparatus (Garzón-Pérez et al., 2020; Zarazúa-Aguilar et al., 2018). Microwave and ultrasound irradiations allow obtaining particles of regular size and reduce crystallization times. With these irradiation techniques, textural and morphological properties of hydrotalcites can be controlled and improved for specific applications such as adsorption.

Another way to improve the adsorption capacity of the hydrotalcites is by the structural reconstruction method, *i.e.*, when hydrotalcites are calcined between 400−600 ºC, the layered structure breaks down, generating mixed oxides that are characterized by higher specific surface area and porosity compared to pristine materials. By rehydrating these oxides in the presence of anions such as those of As, the hydrotalcite regenerates its lamellar structure through the "Memory Effect" (Palomares et al., 2004; Velázquez-Herrera, Sampieri, et al., 2022).

Then, consider the adsorption characteristics of hydrotalcites and the increase of their specific surface area when calcined. In this work, ZnAl hydrotalcites in their mixed oxide form were synthesized by the coprecipitation method at constant pH, assisted by three different crystallization procedures: microwave irradiation, ultrasound irradiation, and synchronous irradiation mode (microwave and ultrasound), to compare their textural and morphological properties generated by the three crystallization methods in the retention of As(III) from aqueous solutions.

2 Methodology

2.1 Synthesis of hydrotalcites and mixed oxides

Hydrotalcite ZnAl was synthesized by coprecipitation at room temperature, constant pH 8 ± 0.5, and N_2 (42 psi) flow to avoid carbonates formation. Determining amounts of Zn (Sigma Aldrich, 98%) and Al (Caledon L.C., 98%) nitrates in a Zn/Al 1M solution with a molar metal ratio x=2.5. This solution was coprecipitated with a NaOH 1M solution (JT Baker, 97%). The resulting suspension was divided into three equal parts; each one was aged in a SBL CW-2000A reactor with microwave (800 W, 2.4 GHz), ultrasound (50 W, 40 kHz), and simultaneous (microwave/ultrasound) irradiation for 5 min. After crystallization treatment, the samples were washed with deionized water and dried in an oven at 70 °C. Subsequently, the samples were calcined at 450 °C in an air atmosphere for 8 h to obtain mixed oxides. Samples were identified with ZnAl to denote the pristine hydrotalcites, followed by U for ultrasound, M for microwave, and UM for synchronous irradiation. Letter C corresponds to calcined samples.

2.2 Materials Characterization

X-Ray Diffraction. The XRD spectra were obtained with a Rigaku Miniflex 600 diffractometer equipped with an X-ray tube with a copper anode with a linear focus of 0.60 W (40 kV and 15 mA). For calcined and uncalcined materials, the measurements were performed from 5 to 80º 2θ using a scan step size of 0.5º/min.

Fourier Transform Infrared Spectroscopy. Infrared spectra were recorded with a Perkin Elmer Spectrum 100 FT-IR with Universal ATR accessory fitted in a wavenumber interval of 4000 to 650 cm^{-1}.

Nitrogen Physisorption. The specific surface areas of the solids were determined by the BET method (Brunauer-Emmet and Teller) using a Gemini VII model 2390-t equipment. The sample pretreatment was carried out at 80°C for 2 h, followed by 12 h at 150°C with an N_2 atmosphere.

Scanning Electron Microscopy. Micrographics were obtained with a JEOL model JSM7800F scanning electron microscope at an acceleration of 3 eV.

2.3 As^{3+} adsorption

2.3.1 Adsorption experiments

The adsorption process was performed as follows: aliquots of 10 mL of an As(III) solution [$NaAsO_2$ (Sigma Aldrich, 90%)] (1 mg/L) were put in contact with 0.01 g of adsorbent for every contact time (30, 60, 90 min), for triplicated. All samples were stirred in a vortex shaker (Vortex-GENIE 2) and were filtered through a 45µm Teflon syringe filter. This procedure was repeated for each sorbent material. The filtered aliquots were quantified by forming iodine and measured by UV-Vis spectroscopy at 460 nm.

The adsorption capacity (q) of the materials was calculated according to the $q = (C_o - C_t)V/m$ *equation*, where V is the volume of the solution in litters, m is the mass of the adsorbent in grams, and C_o is the initial concentration and C_t the concentration at the desired time in mg/mL (Zhou et al., 2017).

2.3.2 Quantification of As^{3+}

The colorimetric detection and quantification of arsenic removal were performed by UV-Vis spectroscopy in a UV-Vis Halo DB-30 equipment with a10 mm quartz cells. The quantification process requires the formation of iodine (Pal et al., 1996; Pasha & Narayana, 2008). KIO_3 (Sigma Aldrich, 99.5%) at 2% and HCl (Fermont, 36.5%) at 1.8 mol/L were used for the formation of iodine. After filtration, 1 mL of KIO_3 and 0.5 mL of HCl were added to every As(III) remaining solution and were subjected to an ultrasonic bath for 5 min, obtaining yellow-colored species.

3 Results

3.1 Materials characterization

The XRD diffraction patterns of synthesized materials are shown in Figure 2. For uncalcined samples (Figure 2A), ZnAl-U, ZnAl-M, and ZnAl-UM samples spectra correspond to the layered zinc-aluminum double hydroxide material according to JCPDS 48-1023 pattern card at 10, 20, 34, 39, 60, and 61° 2θ corresponding to (003), (006), (012), (015), (110), and (113) crystallographic planes; this indicates that the synthesized samples present a rhombohedral crystalline symmetry (Cavani et al., 1991; Wu et al., 2012). Furthermore, the (110) and (113) crystallographic planes were shown as a single peak at 61° 2θ, attributed to an irregular distribution of the cations in the hydrotalcite lamellae (Velázquez-Herrera & Fetter, 2020). Figure 2B shows characteristic signals of ZnO according to the JCPDS 36-1451 reference card; reflections (400), (511), and (440) are observed at 44, 59, and 65° 2θ, corresponding to the spinel ($ZnAl_2O_4$). This indicates that the samples synthesized after calcined have mostly hexagonal crystalline symmetry (Macedo et al., 2017).

Figure 1 X-ray diffraction patterns of A) Hydrotalcites and B) Mixed oxides

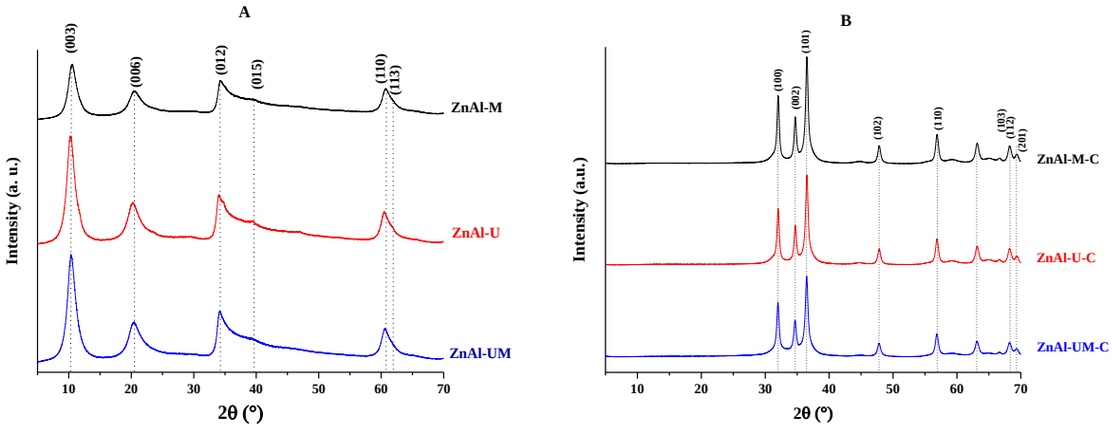

Source: "By the Authors"

Figure 2A shows that the crystalline ordering in the samples was affected by the irradiation type in the crystallization step. ZnAl-M sample exhibit signals with lower intensity and width peak, which corresponds to a lower ordering and crystal size, in contrast with ZnAl-U and ZnAl-UM samples, which present similar intensity and width signals (Paredes-Carrera et al., 2015), indicating that ultrasound irradiation favors the growth and crystals order due to the cavitation effect, which forms points of high pressure, and temperature, favoring the nucleation, orientation, and growth of the crystals in a greater proportion than microwave oven (Garzón-Pérez et al., 2020). In the case of simultaneous irradiation, ultrasonic irradiation was the predominant treatment, probably due to the application of a large amount of vibratory energy to small volumes, limiting the effect of the microwave (Flores-Cantera et al., 2022; Muñoz et al., 2017). In Figure 2B, the effect of the type of irradiation used during the crystallization stage is not appreciable for the mixed oxides.

Table 1 summarizes the structural parameters of the synthesized samples. The crystalline domain was calculated by the Debye-Scherrer equation, $D = 0.94\ \lambda/(\beta \cos\theta)$. Where D is the crystalline domain (nm), λ is the X-ray wavelength (0.15406 nm), β is the width of the peak at half the maximum height (rad), and θ is the Bragg angle (rad). Considering crystals with cubic symmetry and a spherical shape factor (Evans & Slade, 2006). For hydrotalcite, the 003 plane was considered, while for mixed oxides, the 002-plane belonged to ZnO.

Table 1 Structural parameters of samples synthesized

Hydrotalcites					Mixed oxides			
Sample	**$d_{(003)}$ (nm)**	**c (nm)**	**a (nm)**	**D (nm)**	**Sample**	**c (nm)**	**a (nm)**	**D (nm)**
ZnAl-M	0.83	2.56	0.304	4.6	ZnAl-MC	0.52	0.32	17.1
ZnAl-U	0.86	2.61	0.304	4.6	ZnAl-U-C	0.52	0.32	18.1
ZnAl-UM	0.85	2.58	0.304	4.8	ZnAl-UM-C	0.52	0.32	17.5
$d_{(003)}$ is the interlamellar space, a and c are structural parameters ($c = 3d_{(003)}$ and $a = 2d_{(110)}$ for hydrotalcite and, $c = 2d_{(002)}$ and $a = 2d_{(110)}$ for mixed oxides).								

Source: "By the Authors"

The crystalline domain, *D*, for the ZnAl-UM, ZnAl-U, and ZnAl-M samples is close to 4.7 nm, not showing a significant difference for the hydrotalcite, Table 1. Nevertheless, mixed oxides crystalline domains increased to 17.1, 18.1, and 17.5 nm for the ZnAl-M-C, ZnAl-U-C, and ZnAl-UM-C samples, respectively. It is common in mixed oxides as the hydrotalcite structure collapses, promoting an increase in the crystalline domain. Thus, large crystals of ZnO and $ZnAl_2O_4$ are obtained (Cavani et al., 1991). In the mixed oxides, these differences indicate simultaneous irradiation mostly favors the heterogeneous crystalline domain growth due to the cavitation effect of ultrasound. The temperature increase caused by microwaves generated a combined or synergistic effect in the crystalline domains (Garzón-Pérez et al., 2020).

The ZnAl-M, ZnAl-U, and ZnAl-UM samples had an interlayer distance (d_{003}) of 0.84 nm, showing that nitrates are the majority compensating anions. Thus, the lattice parameter *c* is about 2.6 nm, while the reflection (110) related to the lattice parameter *a* is 0.304 nm, corresponding to HT material (Velázquez-Herrera & Fetter, 2020). In the case of mixed oxides, the distance between planes of reflection (002) is related to the lattice parameter *c*. The distance between planes of reflection (110) is related to the lattice parameter *a*, being for all samples c = 0.52 nm and a = 0.32 nm, characteristic of mixed oxides derived from hydrotalcites (Aryanto et al., 2019; Macedo et al., 2017) and similar to zinc oxide.

Figure 3A shows the FTIR spectrum of the ZnAl-U, ZnAl-M, and ZnAl-UM samples. The bands at 3400 cm^{-1} and 1637 cm^{-1} are associated with the stretching and bending mode, respectively, of hydroxyl groups and interlayer water molecules. The strong signal at 1360 cm^{-1} is attributed to nitrates and carbonates in the interlaminar space (Wang et al., 2014). The bands that appear at 400-700 cm^{-1} correspond to the stretching of Zn-O and Al-O (Sommer et al., 2013). Figure 3B shows that the characteristic bands of hydrotalcite disappear for calcined materials, and only bands smaller than 1000 cm^{-1}, corresponding to the vibrations of metals with oxygen, are shown (Kirankumar & Sumathi, 2017).

Figure 3 FTIR spectra of the synthesized samples. A. Hydrotalcites and B. Mixed oxides

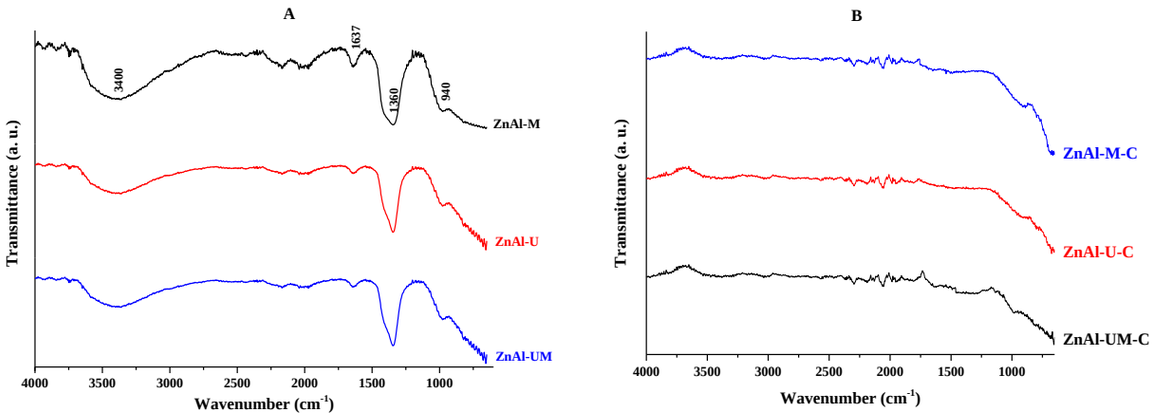

Source: "By the Authors"

The differences observed in transmittance are dependent on the variation of the dipole moment of the molecules, with the coordinate of the vibration mode and the concentration of the molecules in the sample (Wang et al., 2014). Furthermore, samples do not show differences attributed to the crystallization method. Therefore, mixed oxides do not show differences concerning the synthesis method but confirm the correct formation of the hydrotalcite material.

Figure 4 shows the SEM images of the ZnAl-M, ZnAl-U, and ZnAl-UM samples. ZnAl-U sample, Figure 4B, shows a well-defined compact flake-like arrangement of hydrotalcite materials (Bergadà et al., 2007; Velázquez-Herrera et al., 2018). It can be appreciated lamellar sheets are about 50 nm. For the ZnAl-M sample, in Figure 4A, an irregular mix of flakes and chunks of particles on a smooth surface is observable (Zarazúa-Aguilar et al., 2018). Also, a low quantity of flake particles is barely perceptible. Furthermore, for the ZnAl-UM sample, Figure 4C, a homogeneous combination of flakes and chunks is obtained due to the variety of irradiations, which favors the heterogeneity of the particles. Furthermore, can be appreciated the characteristics of ZnAl-M and ZnAl-U samples in different zones.

Figure 4 SEM images of synthesized samples: A. ZnAl-M, B. ZnAl-U, and C. ZnAl-UM. Magnifications are presented in order from top to bottom at 10000 and 25000 X

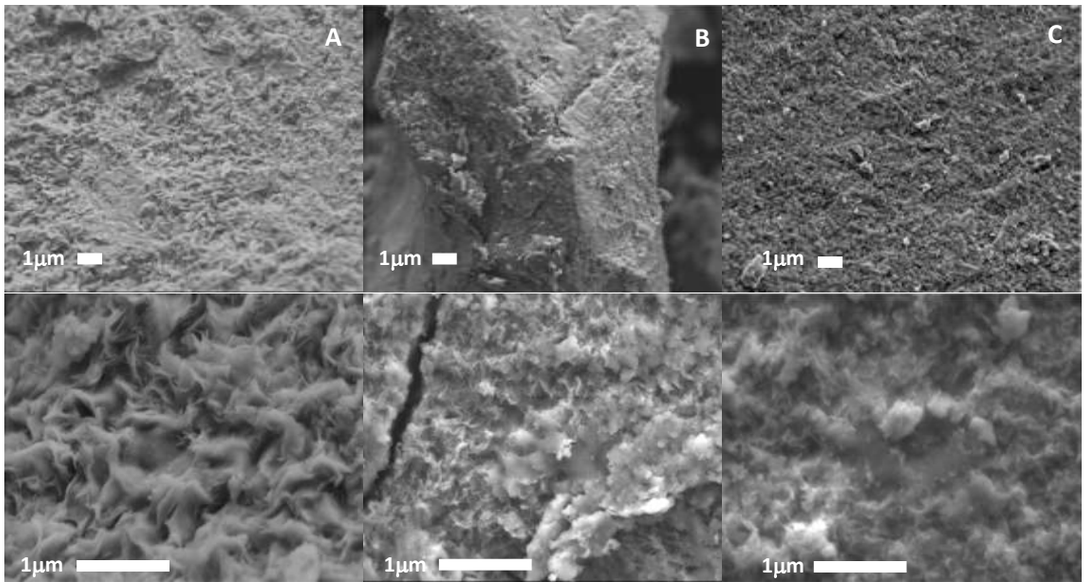

Source: "By the Authors"

The ultrasound irradiation promotes platelet and compact particle arrangements due to the cavitation phenomenon (Morales-Zarate et al., 2018). On the other hand, the microwave method generates uniform surfaces with flakes that are attributed to the diffusion of ions and their rapid integration into the hydrotalcite sheets (Garzón-Pérez et al., 2020). Therefore, simultaneous irradiation (microwave/ultrasound) generates a regular distribution of particles from both irradiations (Garzón-Pérez et al., 2020). In general, morphological differences were attributed to the crystallization method

Figure 5A shows the nitrogen adsorption-desorption isotherms of ZnAl-M, ZnAl-U, and ZnAl-UM samples. All samples showed a Type IV isotherm (IUPAC classification) characteristic of mesoporous materials, with a hysteresis loop of the H1 type (IUPAC classification), which corresponds to aggregates of compact particles of lamellar materials (Seftel et al., 2008; Valente et al., 2009). The specific surface area BET of uncalcined samples was 1 m^2/g. These results agreed with those reported for hydrotalcite containing Zn cations and interlayer nitrate anions (Velázquez-Herrera et al., 2018).

Figure 5 Nitrogen adsorption-desorption isotherms of the samples. A. Hydrotalcites and B. Mixed oxides

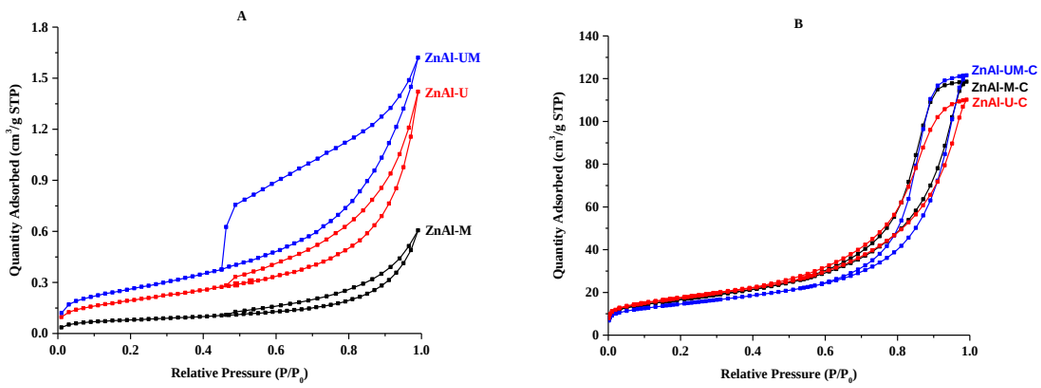

Source: "By the Authors"

Mixed oxides, Figure 5B, showed a Type IV isotherm with a hysteresis loop of the H1 type (IUPAC classification) characteristic of mesoporous materials with large and narrow pore size distributions (Thommes et al., 2015).

The specific surface area BET increased from 1 to 20 m^2/g for the ZnAl-U-C, while for ZnAl-M-C increased to 50 m^2/g. As expected, ZnAl-UM-C surface area increased, achieving a value of 59 m^2/g, due to a combination of crystallization methods, *i.e.*, the well-defined particle arrangement of ZnAl-U-C is damaged after calcination, collapsing the porous hydrotalcite structure generating a compact arrangement and decreasing the specific surface area. However, for the ZnAl-MC sample, the surface particle arrangement is a mix of different irregular particles that, when calcined, preserve a disordered structure producing a large specific surface area (Rodrigues et al., 2003). Furthermore, tiny particles of both irradiation methods should be in a close, freely arranged interaction forming a cloud-like network, Figure 4C, as reported for composite materials where different mixed particles are obtained (Velázquez-Herrera et al., 2020). Thus, simultaneous irradiation in the crystallization step improves the specific surface area due to the agglomerate homogeneous particle distribution. In contrast, pore volume results similar for all ZnAl-M-C, ZnAl-U-C, and ZnAl-UM-C samples, about 0.18 cm^3/g, not showing the influence of the thermal treatment. However, the average pore size increased for the ZnAl-UM-C sample to 6.94 nm; this is in accordance with the specific surface area.

3.2 As (III) adsorption

Figure 6 shows As (III) adsorption capacity for the calcined samples expressed in mg/g *vs*. contact time. In the ZnAl-M-C and ZnAl-U-C samples, the adsorption capacity remained constant at 0.44 and 0.42 mg/g, respectively, while the ZnAl-UM-C sample increased adsorption capacity to about 0.52 mg/g.

Figure 6 The adsorption capacity of mixed oxides for As(III) removal

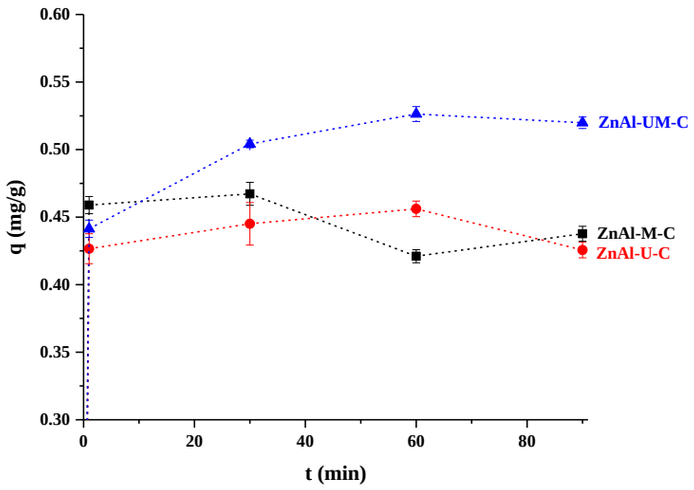

Source: "By the Authors"

The simultaneously irradiated sample (ZnAl-UM-C) showed the highest adsorption capacity for As (III), which is attributed to the specific surface area, 59 m^2/g, and the heterogeneous dispersion of the particles. In addition, the differences found in the adsorption capacity per unit area, 0.021, 0.009, and 0.009 m^2/g for the ZnAl-U-C, ZnAl-M-C, and ZnAl-UM-C samples, respectively, suggest that the ZnAl-U-C sample presents a higher adsorption capacity per unit area than the other samples. This can be attributed to the type of physical adsorption that occurs in the pores, *i.e.*, the isotherms obtained are Type IV, in which the initial monolayer-multilayer adsorption occurs on the mesopore walls and is followed by pore condensation. On the other hand, the relative equality in adsorption per unit area of the ZnAl-M-C and ZnAl-UM-C samples agrees with the isotherms obtained, Figure 5, which are similar. Moreover, it is well known that the hydrotalcite adsorption properties increase considerably if the hydrotalcite is calcined to form mixed oxides (Blanch-Raga et al., 2014).

Therefore, the adsorption capacity can be explained by several factors; the first one is related to the nature of Zn, which, it has been demonstrated that in its oxide form, has a great affinity to adsorb heavy metals (Gu et al., 2020). Secondly, the pore size, which is related to the synthesis method, is observed to increase with simultaneous irradiation, as shown in the SEM images (Figure 4) and verified by nitrogen adsorption-desorption (Figure 5).

Then, simultaneous irradiation generates materials with better textural properties than materials using single irradiation. Consequently, the adsorption of As(III) from aqueous solutions was promoted. Thirdly, the specific surface area allows As(III) ions to distribute on the surface of the mixed oxides. Fourth, it has been reported that particle size influences the adsorption process (Yang et al., 2006). In this case, the calcined samples have a particle size close to 17.5 nm, larger than the uncalcined hydrotalcite, about 4.7 nm. However, the particle arrangement to form the agglomerates was different for each sample, *i.e.*, sample ZnAl-UM-C (Figure 4) showed a combination of two-particle phases generated by both irradiations, Figure 7C, which increases the probability of access of As(III) molecules to the pores of the material.

Ultrasound irradiation generated a uniform distribution of particles, generating a compact agglomerate, Figure 7B, which probably hinders adsorption, whereas microwave irradiation generates not highly ordered agglomerates, Figure 7A. In addition, another aspect being considered is the synthesis process of the hydrotalcite precursors of the mixed oxides. This aspect can be explained in terms of the nature of both irradiations: microwave electromagnetic radiation travels with the speed of light, providing an amount of energy lower than that needed to break a chemical bond (Kumar et al., 2020), which distorts the structure of the material, while ultrasound waves have a high frequency, 40 kHz, which, compared to microwaves is low, so this radiation is confined to the surface of the particles, hindering the cavitation phenomenon (Rezk et al., 2021) and favoring the size of the pores, generating two phases of particles. Thus, the adsorption process contributes to the synthesis method. A simultaneous irradiation method promotes a synergistic state between microwaves and ultrasound in terms of morphology and texture.

Figure 7 Irradiation effect in the particle distribution of the hydrotalcite agglomerate

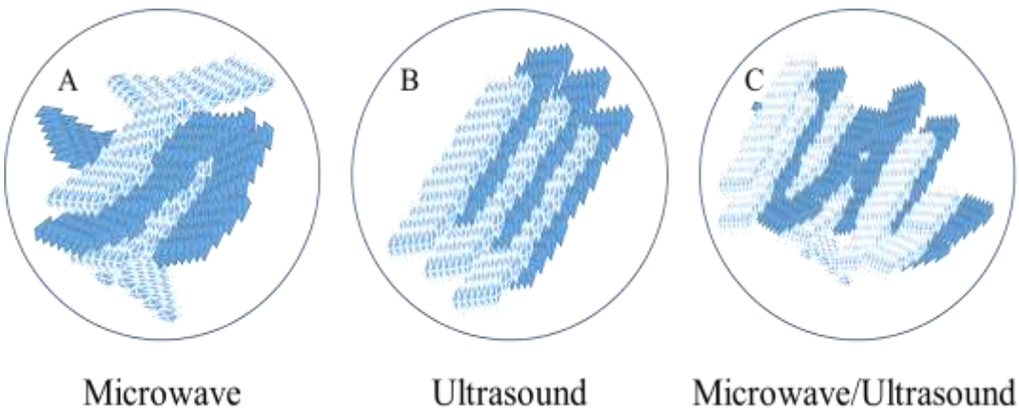

Source: "By the Authors"

To get an idea of the actual adsorption capacity of materials, before calcination and considering the EDS technique, the synthesized ZnAl-hydrotalcites can exchange anions in the interlaminar space up to about 0.41 g_{AsO2}/g_{HT} in the lamellar space, which is higher than what has been reported by other authors (Ramos-Ramírez et al., 2014; Yadav et al., 2017).

4 Conclusion

To sum up, the As(III) removal process resulted from a contribution of particle size, surface adsorption, and the crystallization method (microwave, ultrasound, and simultaneous irradiation). In comparison, microwave irradiation promotes a compact uniform arrangement of particles that increase the specific surface area BET through the improvement of cation diffusion within hydrotalcite lamellae. At the same time, ultrasound generates a distortion in the hydrotalcite lamellae promoting an irregular arrangement of particles that decreases the specific surface area BET, which originated by the cavitation phenom. Therefore, the simultaneous irradiation, microwave/ultrasound, enhances the effect of both irradiations, generating two phases of particles within the agglomerate, which increases the specific surface area BET. This improvement allows obtaining superior materials for the As(III) adsorption process, with which adsorptions of up to 0.52 mg/g in 30 min.

Furthermore, this work provides a simple way to obtain superior materials in a short synthesis time with many potential applications such as catalysts, adsorbents, and others, inclusive in the pharmaceutical industry such as controlled drug liberation.

5 Acknowledgments

The authors thanks to CONACYT and Instituto Politécnico Nacional-SIP project: 20221522 for the financial support and the Centro de Nanociencias y Micro y Nanotecnologías -IPN for technical support.

6 References

Aryanto, D., Marwoto, P., Sudiro, T., Wismogroho, A. S., & Sugianto. (2019). Growth of a -axis-oriented Al-doped ZnO thin film on glass substrate using unbalanced DC magnetron sputtering. *Journal of Physics: Conference Series*, *1191*, 012031. https://doi.org/10.1088/1742-6596/1191/1/012031

Bergadà, O., Vicente, I., Salagre, P., Cesteros, Y., Medina, F., & Sueiras, J. E. (2007). Microwave effect during aging on the porosity and basic properties of hydrotalcites. *Microporous and Mesoporous Materials*, *101*(3), 363–373. https://doi.org/10.1016/j.micromeso.2006.11.033

Blanch-Raga, N., Palomares, A. E., Martínez-Triguero, J., Puche, M., Fetter, G., & Bosch, P. (2014). The oxidation of trichloroethylene over different mixed oxides derived from hydrotalcites. *Applied Catalysis B: Environmental*, *160–161*(1), 129–134. https://doi.org/10.1016/j.apcatb.2014.05.014

Cavani, F., Trifirò, F., & Vaccari, A. (1991). Hydrotalcite-type anionic clays: Preparation, properties and applications. *Catalysis Today*, *11*(2), 173–301. https://doi.org/10.1016/0920-5861(91)80068-K

Conterosito, E., Gianotti, V., Palin, L., Boccaleri, E., Viterbo, D., & Milanesio, M. (2018). Facile preparation methods of hydrotalcite layered materials and their structural characterization by combined techniques. *Inorganica Chimica Acta*, *470*, 36–50. https://doi.org/10.1016/j.ica.2017.08.007

De Gisi, S., Lofrano, G., Grassi, M., & Notarnicola, M. (2016). Characteristics and adsorption capacities of low-cost sorbents for wastewater treatment: A review. *Sustainable Materials and Technologies*, *9*, 10–40. https://doi.org/10.1016/j.susmat.2016.06.002

Deschamps, E., Ciminelli, V. S. T., Weidler, P. G., & Ramos, A. Y. (2003). Arsenic sorption onto soils enriched in Mn and Fe minerals. *Clays and Clay Minerals*, *51*(2), 197–204. https://doi.org/10.1346/CCMN.2003.0510210

Evans, D. G., & Slade, R. C. T. (2006). Structural aspects of layered double hydroxides. In X. Duan & D. Evans (Eds.), *Layered Double Hydroxides* (Vol. 119, pp. 1–87). Springer Berlin Heidelberg. https://doi.org/10.1007/430_005

Flores-Cantera, J., Cruz-Mérida, J. A., Velázquez-Herrera, F. D., Paredes-Carrera, S. P., & Zarazua-Aguilar, Y. (2022). Synchronous microwave and ultrasound irradiation for the synthesis of SBA-15. *MRS Communications*. https://doi.org/10.1557/s43579-022-00190-9

Garzón-Pérez, A. S., Paredes-Carrera, S. P., Martínez-Gutiérrez, H., Cayetano-Castro, N., Sánchez-Ochoa, J. C., & Pérez-Gutiérrez, R. M. (2020). Efecto de la irradiación combinada de microondas-ultrasonido en la estructura y morfología de compuestos tipo hidrotalcita Al/Mg-CH3COO y su evaluación en la sorción de un colorante reactivo. *Revista Mexicana de Ingeniería Química*, *19*(1), 363–375. https://doi.org/10.24275/rmiq/Mat567

Ghashghaee, M., Shirvani, S., Farzaneh, V., & Sadjadi, S. (2018). Hydrotalcite-impregnated copper and chromium-doped copper as novel and efficient catalysts for vapor-phase hydrogenation of furfural: effect of clay pretreatment. *Brazilian Journal of Chemical Engineering*, *35*(2), 669–678. https://doi.org/10.1590/0104-6632.20180352s20160703

Gu, M., Hao, L., Wang, Y., Li, X., Chen, Y., Li, W., & Jiang, L. (2020). The selective heavy metal ions adsorption of zinc oxide nanoparticles from dental wastewater. *Chemical Physics*, *534*, 110750. https://doi.org/10.1016/j.chemphys.2020.110750

Kirankumar, V. S., & Sumathi, S. (2017). Catalytic activity of bismuth doped zinc aluminate nanoparticles towards environmental remediation. *Materials Research Bulletin*, *93*, 74–82. https://doi.org/10.1016/j.materresbull.2017.04.022

Kumar, A., Kuang, Y., Liang, Z., & Sun, X. (2020). Microwave chemistry, recent advancements, and eco-friendly microwave-assisted synthesis of nanoarchitectures and their applications: a review. *Materials Today Nano*, *11*, 100076. https://doi.org/10.1016/j.mtnano.2020.100076

Lima-Corrêa, R. A. B., Castro, C. S., & Assaf, J. M. (2018). Lithium containing MgAl mixed oxides obtained from sol-gel hydrotalcite for transesterification. *Brazilian Journal of Chemical Engineering*, *35*(1), 189–198. https://doi.org/10.1590/0104-6632.20180351s20160146

Macedo, H. P. de, Medeiros, R. L. B. de A., Medeiros, A. L. de, Oliveira, Â. A. S. de, Figueredo, G. P. de, Melo, M. A. de F., & Melo, D. M. de A. (2017). Characterization of ZnAl2O4 spinel obtained by hydrothermal and microwave assisted combustion method: a comparative study. *Materials Research*, *20*(suppl 2), 29–33. https://doi.org/10.1590/1980-5373-mr-2016-0977

Mohan, D., & Pittman, C. U. (2007). Arsenic removal from water/wastewater using adsorbents—A critical review. *Journal of Hazardous Materials*, *142*(1), 1–53. https://doi.org/10.1016/j.jhazmat.2007.01.006

Morales-Zarate, J. A., Paredes-Carrera, S. P., & Castro-Sotelo, L. V. (2018). Mixed oxides of Zn/Al, Zn/Al-La and Zn-Mg/Al: preparation, characterization and photocatalytic activity in diclofenac degradation. *Revista Mexicana de Ingeniería Química*, *17*(3), 941–953. https://doi.org/10.24275/uam/izt/dcbi/revmexingquim/2018v17n3/Morales

Muñoz, M., Moreno, S., & Molina, R. (2017). Oxidative steam reforming of ethanol (OSRE) over stable NiCo–MgAl catalysts by microwave or sonication assisted coprecipitation. *International Journal of Hydrogen Energy*, *42*(17), 12284–12294. https://doi.org/10.1016/j.ijhydene.2017.03.090

Nicomel, N., Leus, K., Folens, K., Van Der Voort, P., & Du Laing, G. (2015). Technologies for arsenic removal from water: current status and future perspectives. *International Journal of Environmental Research and Public Health*, *13*(1), 62. https://doi.org/10.3390/ijerph13010062

Nie, W. (2020). Dynamics analysis of anion exchange in layered double hydroxides. *Brazilian Journal of Chemical Engineering*, *37*(4), 795–803. https://doi.org/10.1007/s43153-020-00070-6

Pal, A., Jana, N. R., Sau, T. K., Bandyopadhyay, M., & Pal, T. (1996). Spectrofluorimetric determination of arsenic in water samples. *Analytical Communications*, *33*(9), 315. https://doi.org/10.1039/ac9963300315

Palomares, A. E., Prato, J. G., Rey, F., & Corma, A. (2004). Using the "memory effect" of hydrotalcites for improving the catalytic reduction of nitrates in water. *Journal of Catalysis*, *221*(1), 62–66. https://doi.org/10.1016/j.jcat.2003.07.013

Paredes-Carrera, S. P., Valencia-Martínez, R. F., Valenzuela-Zapata, M. A., Sánchez-Ochoa, J. C., & Castro-Sotelo, L. V. (2015). Study of hexavalent chromium sorption by hydrotalcites synthesized using ultrasound vs microwawe irradiation. *Revista Mexicana de Ingeniería Química*, *14*(2), 429–436. http://rmiq.org/ojs311/index.php/rmiq/article/view/1267

Pasha, C., & Narayana, B. (2008). Determination of Arsenic in environmental and biological samples using toluidine blue or safranine O by simple spectrophotometric method. *Bulletin of Environmental Contamination and Toxicology*, *81*(1), 47–51. https://doi.org/10.1007/s00128-008-9454-1

Ramos-Ramírez, E., Gutiérrez-Ortega, N. L., Rangel-Porras, G., & Herrera-Pérez, G. (2014). Nano-Mg/Al hydrotalcite: physicochemical characterization and removal of As(III) from aqueous solutions. *MRS Proceedings*, *1616*, imrc2013-s5c-o052. https://doi.org/10.1557/opl.2014.233

Rezk, A. R., Ahmed, H., Ramesan, S., & Yeo, L. Y. (2021). High frequency sonoprocessing: a new field of cavitation-free acoustic materials synthesis, processing, and manipulation. *Advanced Science*, *8*(1), 2001983. https://doi.org/10.1002/advs.202001983

Rodrigues, A. C. C., Henriques, C. A., & Monteiro, J. L. F. (2003). Influence of Ni content on physico-chemical characteristics of Ni, Mg, Al-Hydrotalcite like compounds. *Materials Research*, *6*(4), 563–568. https://doi.org/10.1590/S1516-14392003000400024

Seftel, E. M., Popovici, E., Mertens, M., Witte, K. De, Tendeloo, G. Van, Cool, P., & Vansant, E. F. (2008). Zn–Al layered double hydroxides: Synthesis, characterization and photocatalytic application. *Microporous and Mesoporous Materials*, *113*(1–3), 296–304. https://doi.org/10.1016/j.micromeso.2007.11.029

Sekabira, K., Origa, H. O., Basamba, T. A., Mutumba, G., & Kakudidi, E. (2010). Assessment of heavy metal pollution in the urban stream sediments and its tributaries. *International Journal of Environmental Science & Technology*, *7*(3), 435–446. https://doi.org/10.1007/BF03326153

Sommer, A., Romero, A., Fetter, G., Palomares, E., & Bosch, P. (2013). Exploring and tuning the anchorage of chlorophyllin molecules on anionic clays. *Catalysis Today*, *212*, 186–193. https://doi.org/10.1016/j.cattod.2013.03.014

Thommes, M., Kaneko, K., Neimark, A. V., Olivier, J. P., Rodriguez-Reinoso, F., Rouquerol, J., & Sing, K. S. W. (2015). Physisorption of gases, with special reference to the evaluation of surface area and pore size distribution (IUPAC Technical Report). *Pure and Applied Chemistry*, *87*(9–10), 1051–1069. https://doi.org/10.1515/pac-2014-1117

Valente, J. S., Tzompantzi, F., Prince, J., Cortez, J. G. H., & Gomez, R. (2009). Adsorption and photocatalytic degradation of phenol and 2,4 dichlorophenoxiacetic acid by Mg–Zn–Al layered double hydroxides. *Applied Catalysis B: Environmental*, *90*(3–4), 330–338. https://doi.org/10.1016/j.apcatb.2009.03.019

Velázquez-Herrera, F. D., & Fetter, G. (2020). Hydrotalcites with heterogeneous anion distributions: a first approach to produce new materials to be used as vehicles for a successive delivery of compounds. *Clay Minerals*, *55*(1), 31–39. https://doi.org/10.1180/clm.2020.2

Velázquez-Herrera, F. D., Fetter, G., Rosato, V., Pereyra, A. M., & Basaldella, E. I. (2018). Effect of structure, morphology and chemical composition of Zn-Al, Mg/Zn-Al and Cu/Zn-Al hydrotalcites on their antifungal activity against A. niger. *Journal of Environmental Chemical Engineering*, *6*(2), 3376–3383. https://doi.org/10.1016/j.jece.2018.04.069

Velázquez-Herrera, F. D., González-Rodal, D., Fetter, G., & Pérez-Mayoral, E. (2020). Towards highly efficient hydrotalcite/hydroxyapatite composites as novel catalysts involved in eco-synthesis of chromene derivatives. *Applied Clay Science*, *198*. https://doi.org/10.1016/j.clay.2020.105833

Velázquez-Herrera, F. D., Lobo-Sánchez, M., Carranza-Cuautle, G. M., Sampieri, Á., del Rocío Bustillos-Cristales, M., & Fetter, G. (2022). Novel bio-fertilizer based on nitrogen-fixing bacterium immobilized in a hydrotalcite/alginate composite material. *Environmental Science and Pollution Research*. https://doi.org/10.1007/s11356-021-17943-z

Velázquez-Herrera, F. D., Sampieri, A., Paredes-Carrera, P., & Fetter, G. (2022). Retención de contaminantes aromáticos líquidos mediante hidrotalcitas, óxidos mixtos derivados e hidrotalcitas reconstruidas. *Revista Internacional de Contaminación Ambiental*, *38*, 1–10. https://doi.org/10.20937/RICA.53995

Wang, X., Wu, P., Lu, Y., Huang, Z., Zhu, N., Lin, C., & Dang, Z. (2014). NiZnAl layered double hydroxides as photocatalyst under solar radiation for photocatalytic degradation of orange G. *Separation and Purification Technology*, *132*, 195–205. https://doi.org/10.1016/j.seppur.2014.05.026

Wu, J. S., Xiao, Y. K., Wan, J. Y., & Wen, L. R. (2012). The growth mechanism of hydrotalcite crystal. *Science China Technological Sciences*, *55*(4), 872–878. https://doi.org/10.1007/s11431-012-4766-0

Yadav, M. K., Gupta, A. K., Ghosal, P. S., & Mukherjee, A. (2017). pH mediated facile preparation of hydrotalcite based adsorbent for enhanced arsenite and arsenate removal: Insights on physicochemical properties and adsorption mechanism. *Journal of Molecular Liquids*, *240*, 240–252. https://doi.org/10.1016/j.molliq.2017.05.082

Yang, L., Dadwhal, M., Shahrivari, Z., Ostwal, M., Liu, P. K. T., Sahimi, M., & Tsotsis, T. T. (2006). Adsorption of arsenic on layered double hydroxides: effect of the particle size. *Industrial & Engineering Chemistry Research*, *45*(13), 4742–4751. https://doi.org/10.1021/ie051457q

Zarazúa-Aguilar, Y., Paredes-Carrera, S. P., Valenzuela-Zapata, M. A., & Sánchez-Ochoa, J. C. (2018). Cr (VI) and naftalene simultaneous degradation using layered double hydroxides CuZnGa (Degradación simultánea de Cr(VI) y naftaleno empleando compuestos tipo hidrotalcita CuZnGa). *Revista Mexicana de Ingeniería Química*, *17*(2), 679–691. https://doi.org/10.24275/uam/izt/dcbi/revmexingquim/2018v17n2/zarazua

Zhou, L., Yu, Q., Cui, Y., Xie, F., Li, W., Li, Y., & Chen, M. (2017). Adsorption properties of activated carbon from reed with a high adsorption capacity. *Ecological Engineering*, *102*, 443–450. https://doi.org/10.1016/j.ecoleng.2017.02.036